PAPER

Check for updates

Exploring the antimicrobial potential of chitosan nanoparticles: synthesis, characterization and impact on *Pseudomonas aeruginosa* virulence factors†

Dominik Maršík, [ID] * Olga Maťátková, [ID] Anna Kolková and Jan Masák

The escalating antibiotic resistance observed in bacteria poses a significant threat to society, with the global prevalence of resistant strains of *Pseudomonas aeruginosa* on the rise. Addressing this challenge necessitates exploring strategies that would complement existing antimicrobial agents, *e.g.* by substances mitigating bacterial virulence without eliciting selective pressure for resistance emergence. In this respect, free-form chitosan has demonstrated promising efficacy, prompting our investigation into reinforcing its effects through nanoparticle formulations. Our study focuses on the preparation of chitosan nanoparticles under suitable conditions while emphasizing the challenges associated with stability that can affect biological activity. These challenges are mitigated by introducing quaternized chitosan, which ensures colloidal stability in the culture media. Our approach led to the production of trimethylchitosan nanoparticles with a median size of 103 nm, circularity of 0.967, and a charge of 14.9 $\pm$ 3.1 mV, stable within a one-month period in a water stock solution, showing promising attributes for further valorization. Furthermore, the study delves into the antimicrobial activity of trimethylchitosan nanoparticles on *Pseudomonas aeruginosa* and confirms the benefits of both nanoformulation and modification of chitosan, as our prepared nanoparticles inhibit 50% of the bacterial population at concentration $\geq$160 mg L^{-1} within tested strains. Additionally, we identified a concentration of 5 mg L^{-1} that no longer impedes bacterial growth, allowing reliable verification of the effect of the prepared nanoparticles on *Pseudomonas aeruginosa* virulence factors, including motility, protease activity, hemolytic activity, rhamnolipids, pyocyanin, and biofilm production. Although trimethylchitosan nanoparticles exhibit promise as an effective antibiofilm agent (reducing biofilm development by 50% at concentrations ranging from 80 to 160 mg L^{-1}) their impact on virulence manifestation is likely not directly associated with quorum sensing. Instead, it can probably be attributed to non-specific interactions with the bacterial surface. This exploration provides valuable insights into the potential of quaternized chitosan nanoparticles in addressing *Pseudomonas aeruginosa* infections and underscores the multifaceted nature of their antimicrobial effects.

Introduction

Chitosan (CS) is a natural biopolymer consisting of D-glucos-amine and *N*-acetyl-D-glucosamine units connected through β-1,4-glycosidic bonds. It is derived from the naturally occurring chitin polymer through a process of partial *N*-deacetylation. Chitin is abundantly found in nature, notably in the exoskele-tons of crustaceans and insects, and the cell walls of fungi.[1] During the *N*-deacetylation process, secondary amine groups become exposed, exhibiting a pK_a value of approximately 6.5. In acidic solutions below this pH, these amine groups become fully protonated, resulting in a positive charge.[2]

CS as a bulk material has received approval in both the EU and USA for dietary and wound dressing applications.[3] Currently, a multitude of investigations is underway, exploring CS in the form of nanoparticles (NPs) for the targeted delivery of therapeutic agents, including proteins, vaccines, and nucleic acids.[4] With its biocompatibility, biodegradability, and adsorption properties, chitosan serves as an integral compo-nent in composite materials, contributing to the acquisition of unique characteristics through diverse combinations.[5–8] Furthermore, CS has demonstrated antimicrobial and anti-biofilm properties. In the case of G-bacteria, these effects are attributed to the chelation of bivalent ions (Ca^{2+} and Mg^{2+}) from the bacterial outer membrane and electrostatic interactions

Department of Biotechnology, University of Chemistry and Technology, Technická 5, Prague 6, Prague, 166 28, Czechia. E-mail: marsikd@vscht.cz

with the anionic components of lipopolysaccharides. Next, CS has been shown to disrupt the inner membrane of bacteria. These interactions result in the impairment of cell wall integrity, hindered transport processes, and loss in intracellular materials, and facilitate the entry of CS into the cytosol, where it can interfere with nucleic acid synthesis.[9] These properties are particularly intriguing in the context of the escalating problem of antimicrobial resistance.

The unique attributes of nanoparticles, such as their increased surface area-to-volume ratio and surface charge density compared to the bulk material, enable them to interact more effectively with the negatively charged bacterial cell envelopes. This can lead to the formation of an impermeable layer of CS-NPs around the bacterium, thereby preventing transport through the outer membrane of G-bacteria.[10] Additionally, the nanoscale dimensions may promote biocompatibility and reduce unwanted interactions with the immune system.[11] As a result, we have embarked on an investigation into the antimicrobial effects of CS-NPs using a model microorganism for biofilm formation, *Pseudomonas aeruginosa* (PA). It is worth noting that since 2017, a carbapenem-resistant strain of PA has been included on the WHO list of microorganisms for which new treatment strategies are urgently needed,[12] particularly strategies that do not exert selective pressure for the emergence of resistance.[13] Given the evolutionary conservation of the essential negative charge of microbial cell envelopes, it is unlikely that bacteria will develop resistance to CS-NPs.[2] Furthermore, there is evidence that CS interferes with the PA quorum sensing (QS) system.[14] QS is a bacterial communication mechanism mediated by small, membrane-diffusing signalling molecules that are released into the local environment. QS activation is contingent upon reaching a threshold cell concentration, which subsequently regulates gene expression and shapes specific bacterial phenotypes. These changes are pivotal for the bacteria's ability to thrive in competitive environments, adapt to metabolic demands, and modulate the production of virulence factors, including elastase, exotoxin A, pyocyanin, lipase, pyoverdine, lectins, and, importantly, biofilm formation.[15,16] The biofilm formation process relies on the essential involvement of type IV pili and flagella motility.[17] Formed biofilm matrices, comprising negatively charged elements such as extracellular polymeric substances (EPS), eDNA, and proteins, represent additional targets for electrostatic interactions with CS-NPs, aided by their nanoscale dimensions penetrating inside.[18]

In the realm of CS-NP synthesis through the ionic cross-linking methods, the crucial factor is the positive charge inherent to CS. These techniques rely on electrostatic interactions with either negatively charged macromolecules or anionic cross-linking agents.[19] Among the various employed techniques, the most widely adopted is the ionic gelation process using trivalent tripolyphosphate anions (TPP).[20] This method is advantageous for its ease of execution, absence of undesirable side reactions, utilization of aqueous solutions, non-toxicity of TPP, which makes it acceptable as a food additive by the FDA,[21,22] and the absence of high-temperature requirements, making it suitable for encapsulation of thermosensitive active

compounds.[23] However, despite the relative simplicity of synthesizing CS-NPs, the establishment of appropriate reaction conditions remains a challenging task. This challenge arises from the intricacies associated with various factors such as the initial concentration of reagents,[24,25] the ratio of reactants,[26] the presence or absence of salts in the reaction medium,[27] and the molecular weight and degree of CS deacetylation.[28,29] Furthermore, CS-NPs prepared through ionic gelation utilizing TPP often exhibit a broad size distribution and limited colloidal stability.[30] This instability poses a challenge, particularly when evaluating the antimicrobial effects of CS-NPs or assessing their cytotoxicity. Of note, standard culture media used for culturing model pathogenic microorganisms and tissue cells, such as LB medium, TSB medium, and DMEM medium, typically maintain a pH range from 6.5 to 7.5. *In vitro* tests designed for the study of antimicrobial effects and cytotoxicity primarily rely on the inherent buffering capacity of these solutions and often lack a more sophisticated system capable of maintaining a constant pH during cultivation and as a result pH can fluctuate during cultivation due to the influence of metabolites.[31] Upon introduction into the culture medium, CS-NPs may undergo deprotonation due to changes in pH, resulting in reduced electrostatic repulsion and decreased affinity between amino groups and TPP. The elevated temperatures typically employed (usually 37 °C) for cultivation of pathogenic microorganisms or tissue cultures further exacerbate the aggregation of CS-NPs.[32]

To mitigate the challenges posed by deprotonation, quaternization of chitosan's amino groups can be employed. This modification ensures the retention of a positive charge even under neutral and slightly alkaline pH conditions, expanding the solubility range of CS. This increased solubility arises from the substitution of primary amines with alkyl groups, which prevent the formation of hydrogen bonds between the amines and the hydroxylic groups in the CS chain.[33] Additionally, nanoparticles prepared from quaternized CS using TPP as a crosslinker exhibit low cytotoxicity, akin to those derived from unmodified CS.[1]

Results and discussion

Preparation of CS/TMC-NPs for antimicrobial applications

Our objective was to craft CS-NPs possessing characteristics suitable for biomedical applications, including nanoscale size, a narrow size distribution, regular spherical morphology, long-term stability, and stability in culture media to facilitate the evaluation of the antimicrobial efficacy of CS in nanoparticle form against the pathogenic bacterium PA. In this study, two types of chitosan were used, specifically CS representing unmodified chitosan and TMC denoting quaternized chitosan by means of trimethylation.

In the initial phase of screening for suitable preparation conditions of CS/TMC-NPs using the ion-crosslinking method, we monitored parameters such as hydrodynamic size, polydispersity index, and ζ-potential. In a study conducted by Sreekumar *et al.*,[28] it was found that the primary factor influencing the mean hydrodynamic size, when transitioning from nano- to micrometer-sized CS-NPs prepared *via* ionic gelation,

was the input concentration of CS. However, the substantial alterations in particle size were observed within a broad input CS concentration range, spanning from 0.10 mg mL^{-1} to 5.00 mg mL^{-1}. In our narrower range of CS input concentration (ranging from 0.50 to 1.00 mg mL^{-1}), considered as an appropriate range for production of nanosized particles, we observed that changes in the input concentration had a less pronounced effect on the resulting nanoparticle size (Fig. 1). Nevertheless, a slight increase in the hydrodynamic size of the particles was noted with increasing reactant concentrations, particularly in an acetate buffer. This phenomenon aligns with observations made in a study conducted by Liu et al.[24] and applies within the appropriate zone of TPP and CS mass ratios. By appropriate zone we mean the point where additional increases in the reaction ratio lead to a significant escalation in the mean hydrodynamic size of particles, as determined by dynamic light scattering (DLS), indicating system aggregation. In the case of CS-NPs, this zone was confined up to a mass reaction ratio of 0.33, with the exception of an input concentration of 0.50 mg mL^{-1} when diluted acetic acid was used as a solution for CS-NP synthesis. With the further addition of TPP, the aggregate

formation becomes apparent from the increase in both hydrodynamic size and PDI (polydispersity index) values. Thus, in our assessment of the parameters suitable for CS-NP preparation, we attach greater significance to the reaction ratio m_{TPP}/m_{CS} than to the input concentration of CS itself. This emphasis on the reaction ratio stems from our hypothesis that, at the verge of aggregation, the maximum conversion of CS into nanoparticles is achieved. Subsequent to the further addition of TPP, the CS-NPs become interconnected through inter-crosslinks between various polymer chains.[27]

As previously mentioned, when the input concentration of CS was 0.50 mg mL^{-1} in an aqueous solution containing acetic acid, the zone of appropriate TPP and CS mass ratio was limited to a value of 0.25. It's important to note that while this shift did not occur in the acetate buffer, the PDI index exhibited a significant increase in comparison to concentrations of 0.75 mg mL^{-1} and 1.00 mg mL^{-1}. Evidently, at this particular input concentration of CS, particles with a broader size distribution are formed and such high PDI values may also indicate the presence of aggregates. Liu and Gao[24] suggest that this phenomenon may be attributed to changes in spatial
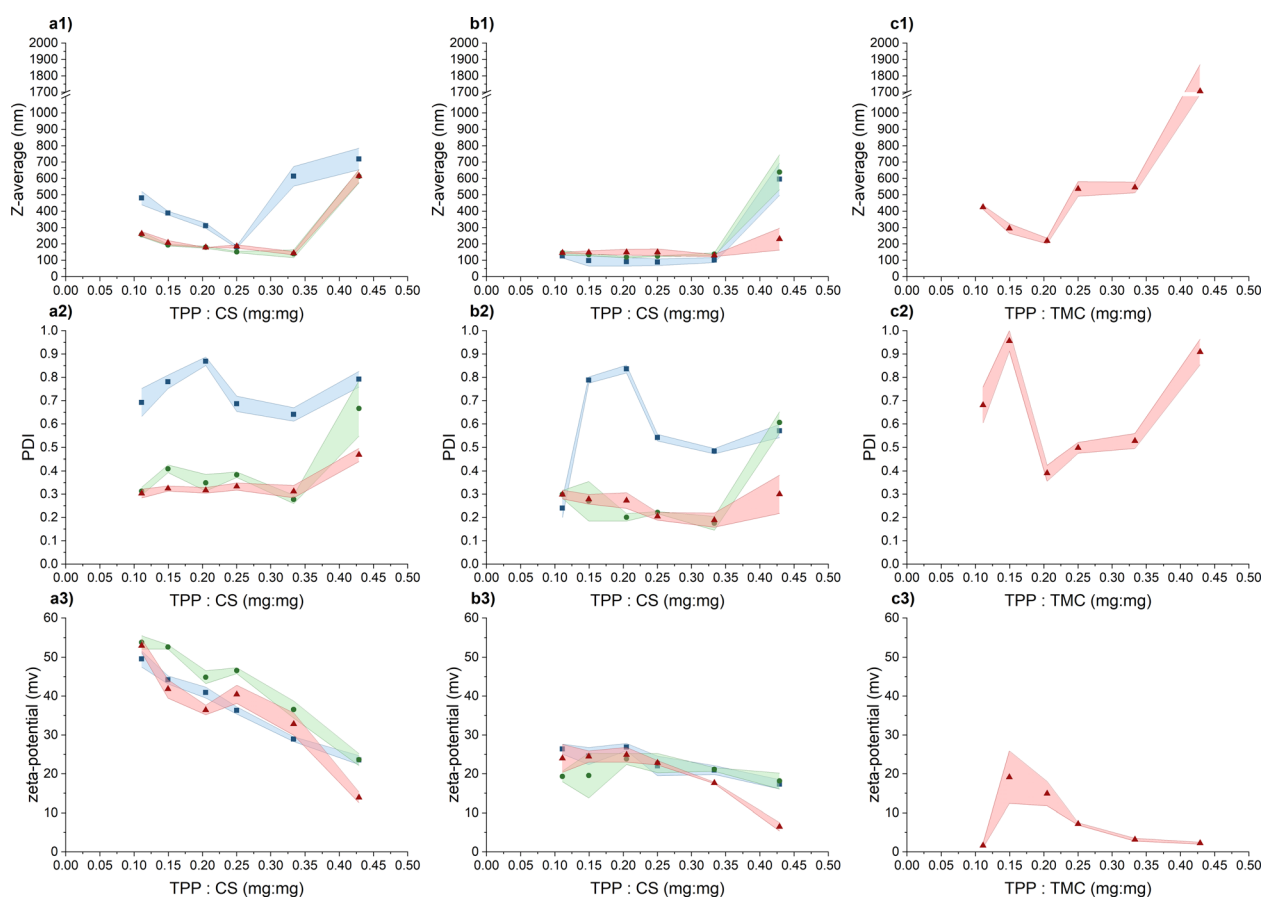
Fig. 1 Exploring suitable conditions for the CS/TMC-NP preparation by comparing the intensity weighted mean hydrodynamic size (Z-average), polydispersity index (PDI) and zeta-potential values based on the TPP and CS/TMC mass ratio. The appropriate zone of TPP and CS/TMC mass ratio is considered up to the point of significant increase in the mean hydrodynamic size as a result of the increasing concentration of the cross-linking agent (TPP): (a) CS in diluted acetic acid; (b) CS in acetate buffer; (c) TMC in UPW; (1) intensity weighted mean hydrodynamic size; (2) polydispersity index; (3) ζ-potential. Chitosan input concentrations: ■ 0.50 mg mL^{-1}; ● 0.75 mg mL^{-1}; ▲ 1.00 mg mL^{-1}. Coloured areas represent standard deviation values of 3 independent repetitions.

interaction distances or alterations in the inner structure of the particles, such as increased compactness of the CS molecule chain. The increasing ionic strength of the medium leads to the screening of electrostatic charges within the CS chains by salts, leading to its enhanced compactness and flexibility.[34,35] This possibly elucidates why the use of an acetate buffer generally resulted in particles with a smaller hydrodynamic size that in a dilute acetic acid solution. This observation aligns with findings by Jonassen *et al.*,[27] who noted a decrease in particle size after the addition of 0.05 M NaCl at all tested TPP : CS ratios. The general decrease in PDI values following the addition of sodium acetate can be attributed to a combination of the reduction in the intrinsic viscosity of CS and slower kinetics of the CS-NP formation process, a trend observed by Sawtarie *et al.*[36] After the addition of NaCl, the slow kinetics allow for a more thorough mixing of CS and TPP before ionic gelation, resulting in a more uniform rate of CS-NP formation and narrow size distribution.

When evaluating the ζ-potential values (Fig. 1), the anticipated decrease in the average value with the increasing concentration of negatively charged TPP was confirmed.[30] In the acetic acid aqueous solution, the ζ-potential values within the appropriate mass ratio zone range from 32.8 ± 2.9 mV to 53.8 ± 1.7 mV, indicating a high level of colloidal stability. In the acetate buffer, the measured values were lower, ranging from 17.7 ± 0.2 mV to 26.4 ± 1.3 mV, signifying relatively stable to moderately stable colloidal stability.[37] Beyond the appropriate mass ratio zone, when TPP is in excess, the surface charge density of the particles decreases to a point where these nanoparticles lose their stability, becoming more prone to mutual interactions and aggregation.[30] The lower values recorded in the acetate buffer are likely a result of salt-induced charge screening,[24] which also leads to a slight reduction in ζ-potential values compared to the acetic acid aqueous solution.[27]

Subsequently, transmission electron microscopy (TEM) was employed to assess the morphological characteristics of CS-NPs synthesized in both diluted acetic acid and acetate buffer solutions. Specific samples were chosen based on DLS data at an input CS concentration of 1 mg mL^{-1} within the mass ratio of 0.33, which remained within the suitable reactant mass ratio zone (Fig. 1). Fig. 2 illustrates the irregular morphologies of CS-NPs produced in acetic acid aqueous solution, alongside the presence of microparticles in the sample. The utilization of acetate buffer as a medium for nanoparticle synthesis led to improved circularity and size distribution of CS-NPs. The median size and circularity were determined to be 30 nm and 0.986, respectively (Fig. 3). Image analysis was not performed for CS-NPs prepared in the acetic acid aqueous solution due to their unsatisfactory morphology and wide size distribution, rendering them unsuitable for consideration as potential antimicrobial agents.

In response to the marginal impact of CS input concentration on NP preparation within our tested range, TMC-NPs were synthesized at a fixed input concentration of 1 mg mL^{-1}. The zone of appropriate reactant mass ratios differed from that observed for CS-NPs, particularly in the case of TMC-NPs, where it was identified at a value of 0.20 (Fig. 1). Both CS and TMC
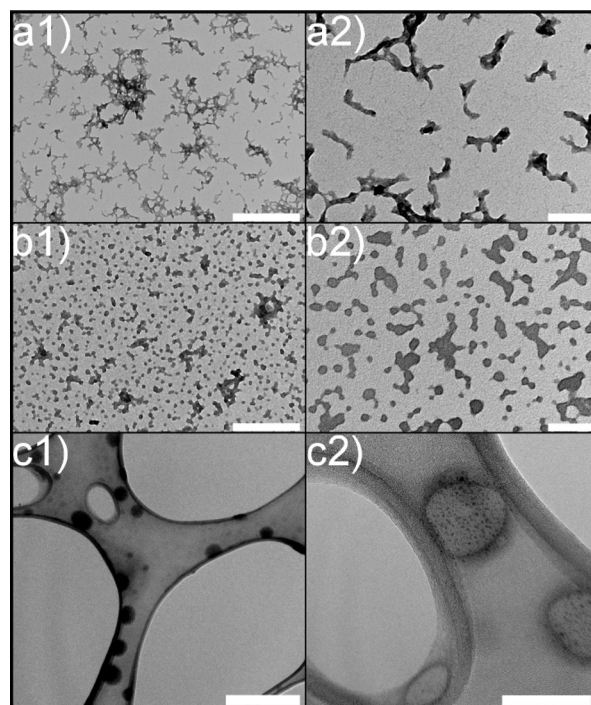

Fig. 2 Morphology of chitosan nanoparticles: (a) CS in diluted acetic acid; (b) CS in acetate buffer; (c) TMC in UPW; (1) scale bar represents 500 nm; (2) 100 nm scale.
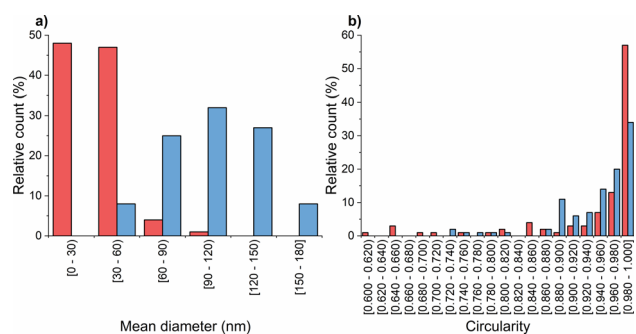

Fig. 3 Chitosan nanoparticle characteristics: (a) size; (b) circularity of CS-NPs; TMC-NPs.

used in our work were LMW chitosans, which under the given conditions exhibit a similar proportion of protonated amines (CS 75–85% deacetylated, TMC > 70% quaternized), consequently providing a similar quantity of available positive charges for interaction with TPP. However, this observed shift in the appropriate ratio might be attributed to steric hindrance introduced by the methyl groups within the TMC structure. This effect aligns with previous observations made by Kiang *et al.*,[38] who explored the impact of chitosan deacetylation levels on the synthesis of CS-NPs using DNA as the negatively charged molecule for ionic crosslinking. The chosen appropriate reaction ratio between TMC and CS closely coincides with those employed by Geçer *et al.*[39] and Sayın *et al.*[40] in their respective studies.

The resulting ζ-potential up to $m_{TPP}/m_{TMC} = 0.20$ varied from 1.6 ± 0.6 mV to 19.1 ± 6.7 mV (Fig. 1), indicating a range from highly unstable to relatively stable nanoparticles (NPs).[37] In general, higher values of the mean hydrodynamic size and polydispersity index (PDI), when compared to the corresponding concentration and reaction mass ratio of CS (Fig. 1), suggest that the prepared TMC-NPs are generally larger than CS-NPs, and the synthesis process is more prone to aggregate formation. Image analysis revealed that TMC-NPs, prepared at a reaction ratio of 0.20, exhibited a median size of 103 nm and a circularity of 0.967 (Fig. 3). In comparison to CS-NPs (prepared in acetate buffer), they displayed a broader size distribution but generally had a narrower circularity distribution. The TMC-NPs prepared in this study exhibit a distinctive morphology and size profile, setting them apart from existing literature on CS-NP preparation (Fig. 2). Our TMC-NPs align with the criteria for biomedical applications[41] while adhering to the European Commission's recommended definition of nanomaterials, which classifies nanomaterials as such when 50% or more of their constituent particles fall within the size range of 1–100 nm.[42]

In the context of TMC-NPs and CS-NPs in an acetate buffer solution, evaluating their stability in culture media is a pivotal step for the subsequent assessment of the antimicrobial capacity of these systems. Luria Bertani (LB) medium serves as a common culture medium for conducting antimicrobial tests against PA.[43] After preparing blank samples containing LB media and CS/TMC-NPs at concentrations ranging from 5 mg L^{-1} to 160 mg L^{-1}, we observed the formation of aggregates within several minutes in the sample containing CS-NPs. In contrast, a stable suspension was formed with TMC-NPs (Fig. S1†). Given the relatively low ζ-potential values of TMC-NPs, we also examined the stability within the stock solution stored at 4 °C (Fig. 4). Over a one-month period, there were no discernible changes in the mean hydrodynamic size or ζ-potential, signifying the absence of time-dependent system destabilization.[44] Consequently, we opted to conduct a antimicrobial test with TMC-NPs.
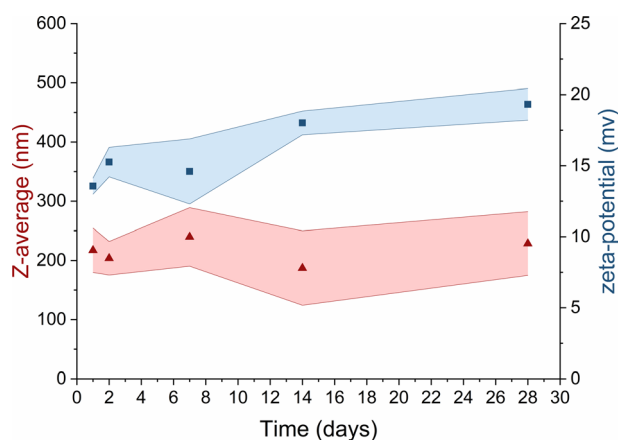

Fig. 4 Long-term stability of TMC in UPW ▲ mean hydrodynamic size; ■ ζ-potential. Coloured areas represent the standard deviation values of 3 independent repetitions.

Antimicrobial activity of TMC-NPs against PA planktonic cells – MIC and sub-MIC determination

TMC-NPs hold considerable potential as an antimicrobial system, particularly in combination with other antimicrobial agents, thereby presenting viable prospects for utilization in various biomedical fields.[45] Furthermore, we investigated their influence on the virulence of PA. To achieve this, it was imperative to identify a sub-MIC concentration, defined as a concentration that does not impede the growth kinetics of PA, as a virulence manifestation is contingent upon cell concentration.[46] The sub-MIC concentration of TMC-NPs was consistently identified at 5 mg L^{-1} across all three tested PA strains, as illustrated in Fig. 5. Beyond this threshold, we observed a progressive enhancement of the antimicrobial effect with increasing TMC-NP concentrations. The MIC$_{50}$ values were determined to be 160 mg L^{-1} for strains ATCC 155442 and ATCC BAA-47 (PA01). However, in the case of strain ATCC 10145, the MIC$_{50}$ value exceeded 160 mg L^{-1}.

In a study by Boudouaia *et al.*,[47] the effectiveness of a CS solution (DDA 95%, LMW) was assessed using evaluation of inhibition zones on agar plates. Interestingly, they observed complete resistance of PA to concentrations up to 0.50% CS solution. In another agar plate experiment, wherein CS (LMW) at a concentration of 1000 mg L^{-1} was evaluated by measuring the relative inhibition time for visible PA colonies (ATCC 27853) on agar plates, the incubation phase was extended by 5 h to over 85 hours, depending on the *N*-acetylation degree of CS.[48] In a particularly promising study by Tin *et al.*,[49] the antimicrobial effect was quantified as MIC, defined as the lowest CS concentration that prevented visible PA growth. CS (DDA 75–85%, LMW) exhibited impressive results, with an MIC of 32 mg L^{-1} for four PA strains (ATCC15279, PA01, PT121, and PT149). Conversely, in a study conducted by Liu *et al.*,[50] MIC values for PA (PA01) in response to water-soluble chitosan chloride (91% DDA, LMW) and sulfonated chitosan (86% degree of substitution, LMW) were found to be notably higher, specifically 1000 mg L^{-1}. In addition to sulfonation, a general enhancement in antimicrobial properties was observed after CS methylation. However, with PA (ATCC 43300), the MIC values for TMC$_{NH_2/TM}$ with different degrees of substitution ranged from 1024 mg L^{-1} to ≥ 8192 mg L^{-1}.[51] Similarly, Maisetta *et al.*[52] examined the effect of quaternized chitosan (80% degree of substitution, LMW) against four PA strains (W4, CVC02118, BAL091, and ATCC 27853) and reported MIC values ranging from 2500 to 5000 mg L^{-1}.

The antimicrobial activity of CS and its derivatives, including NPs, is contingent on a complex interplay between intrinsic factors and environmental conditions.[48,53] This multifaceted nature is reflected in the variability in reported antimicrobial effects against PA across the existing literature. In our study, we observed a relatively low MIC$_{50}$ for TMC-NPs, suggesting their effectiveness against PA. This efficacy may be attributed to the maintenance of a stable TMC-NP suspension in LB medium (Fig. S1†). Conversely, the formation of aggregates within unmodified CS-NPs could explain the high concentrations required to inhibit PA in discussed studies, possibly due to the
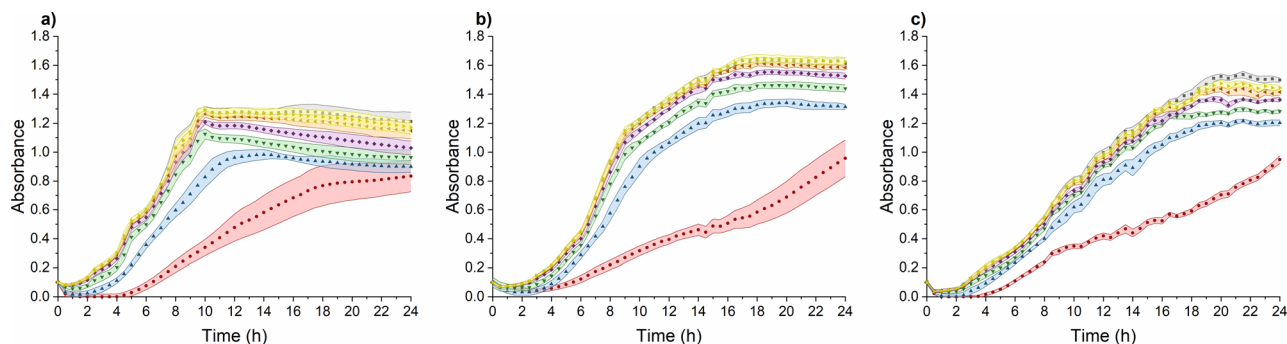
Fig. 5 Effect of TMC-NPs on PA suspension growth: (a) ATCC 10145; (b) ATCC 15442; (c) ATC BAA-47 (PA01). Concentration (mg L^{-1}) of TMC in TMC-NPs: ■ 0; ▶ 5; ◀ 10; ◆ 20; ▼ 40; ▲ 80; ● 160. Coloured areas represent standard deviation values of five parallel and three independent experiments.

susceptibility of unmodified CS to aggregation after transfer into culture media. This finding aligns with Salis et al.,[54] who reported the aggregation of chitosan-modified silica nanoparticles in culture media, leading to reduced uptake by mouse fibroblasts. Additionally, previous studies have demonstrated that methylation of CS enhances interactions with biological membranes, leading to membrane lysis,[55] which may contribute to the effectiveness of our TMC-NPs. Furthermore, we hypothesize that the permanent charge conferred by methylation could enable TMC-NPs to penetrate the internal environment of bacterial cells,[56] interact with nucleic acids, and thereby enhance antimicrobial efficacy compared to CS-NPs. Indeed, methylation-mediated penetration into the internal cellular environment has been demonstrated in tissue cultures,[57] and the size of our 103 nm TMC-NPs indicates suitability for efficient transport through biological membranes.[58] However, the currently prevailing understanding of CS action involves primary interactions with bacterial envelopes and their disruption, potentially leading to interactions with internal components.[59–61]

Antimicrobial activity of TMC-NPs against PA biofilm cells – MBIC determination

CS is recognized in the literature for its antimicrobial properties, particularly as an antibiofilm agent. Often higher concentrations are required to inhibit the planktonic type of growth of PA compared to concentrations sufficient to impede the adhesion and subsequently inhibit biofilm development.[62,63] Our study aligns with this trend, revealing MBIC$_{50}$ values of 80 mg L^{-1} for ATCC 10145 and ATCC BAA-47 (PA01), and 160 mg L^{-1} for ATCC 15442 (Fig. 6).

The initial adhesion of PA relies on surface virulence factors such as flagella, pili, lipopolysaccharides (LPS), and exopolysaccharides. The negatively charged bacterial cell surface facilitates electrostatic interactions with TMC-NPs, sterically hindering adhesion.[64] Intriguingly, a decrease of approximately 15% occurred at a sub-MIC concentration of 5 mg L^{-1} for all three strains, indicating that the effect is not only related to growth inhibition. In addition to steric hindrance to adhesion, this may be attributed to interference with the quorum sensing

system, implicated in biofilm formation, as hypothesised by Piras et al.[62] Their study demonstrated that quaternized chitosans inhibited total PA (ATCC 27853) biofilm biomass by 50% in a concentration range of 37–150 mg L^{-1} in dependence on derivatives tested. Those concentrations were not effective against the planktonic type of growth. Furthermore, interference with quorum sensing was supported by studies revealing downregulation of *lasR* and *rhlR* genes after exposure of PA to CS, which govern the PA quorum sensing system.[14,52,65,66] In contrast, Maisetta et al.[52] observed an increase in PA total biofilm biomass (W4, CVC02118, BAL091, ATCC 27853) in response to the sub-MIC concentration (37 mg L^{-1}) of quaternized chitosan. The benefit of quaternization is evident when comparing the present study with the findings of Liu et al.,[50] who observed a decline in the PA01 biofilm metabolic activity by 50% when treated with water-soluble chitosan chloride (91% DDA, LMW) or sulfonated chitosan (86% degree of substitution, LMW) at a concentration of 1000 mg L^{-1}. Additionally, following CS
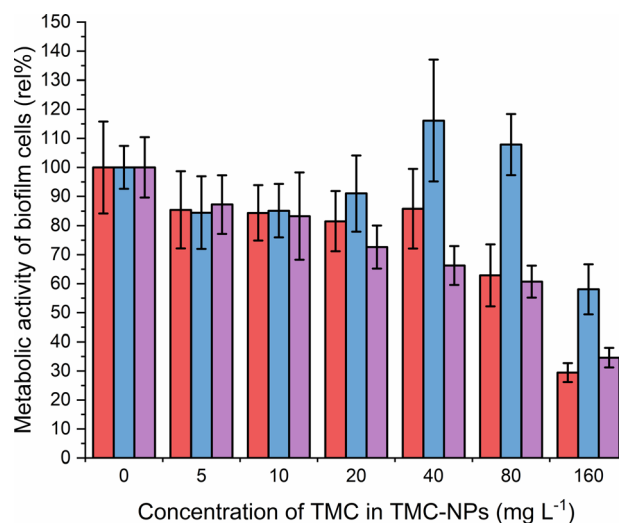

Fig. 6 Effect of TMC-NPs on adhering PA cells ▬ ATCC 10145, ▬ ATCC 15442, and ▬ ATCC BAA-47 (PA01) in comparison to the untreated control. The presented values are a result of eight parallel and three independent repetitions.

treatment, disruptions in biofilm structural integrity and a reduction in EPS production were observed in their study. Consequently, an alternative action of TMC-NPs at higher concentrations could be electrostatic interactions with biofilm components such as exopolysaccharides or extracellular DNA. The impact of CS-NPs, prepared by CS (LMW) ionotropic gelation, on biofilm eradication was visually confirmed by Rivera Aquayo *et al.*[64] at a concentration of 280 mg L^{-1}. Additionally, the impact of CS in the form of complex nanoparticles has been studied against PA. For instance, NPs synthesized through ionic complexation of CS using alginic acid as a gel core were visually observed to affect mature biofilm at 40 mg L^{-1}.[67] Highly effective complex CS-NPs, incorporating the polycationic pyrrole polymer (PPy), were successfully developed in a study by Khan *et al.*[63] The decrease of total biofilm biomass by 50% was determined from 16 mg L^{-1}. However, it is important to note that this effect was not solely attributed to chitosan, as PPy at corresponding concentrations exhibited similar actions against PA adhesion. In conclusion, the TMC-NPs prepared in this study exhibit efficacy at relatively low concentrations, serving as an effective system against PA adhesion and biofilm development.

Effect of TMC-NPs against PA virulence factors

Effect of TMC-NPs' sub-MIC on PA cells' motility. PA exhibits three distinct types of motility—swimming, twitching and swarming. Swimming motility, dependent on flagella, involves movement in aqueous environments up to an agar concentration of 0.3%.[68] PA (wild type) utilizes its approximately 10 μm long flagellar filament located on the bacterial pole for this form of motility.[69,70] The poles of the bacterial body are also equipped with type IV pili, approximately 2.5 μm in length, facilitating surface motility.[71] These retractile extracellular filaments drive twitching motility.[72] The final type, swarming motility, is characterized by fast and coordinated group movement on a semi-solid surface, a consequence of mutual intercellular interaction.[73] This social movement allows bacteria to quickly colonize surfaces, ultimately leading to biofilm formation.[74] Swarming motility is a complex mechanism regulated by numerous cooperating genes,[75] as indicated by differential gene expression. The cells at the tendril tip are generally responsible for spreading, while those in the swarm centre prepare for permanent surface settlement.[73] Besides the flagellum and type IV pili, swarming motility is also influenced by rhamnolipid production.[76,77]

The impact of quaternized chitosan on PA motility was observed, as seen in the strains ATCC 27853 and B910, where swarming motility was reduced by 52% and 40%, respectively, at a concentration of 620 mg L^{-1}.[52] In another study involving strain PA KCTC1637, chitosan nanoparticles were found to be more effective against swimming motility, while swarming motility was more inhibited by free chitosan, within a concentration range of 32–256 mg L^{-1}.[63] In our study (Fig. 7a), at a concentration of 5 mg L^{-1} TMC-NPs, the swimming diameter was slightly reduced in all three strains; however, twitching motility was minimally affected. In the case of swarming motility, a reduction was observed in the context of PA01, while
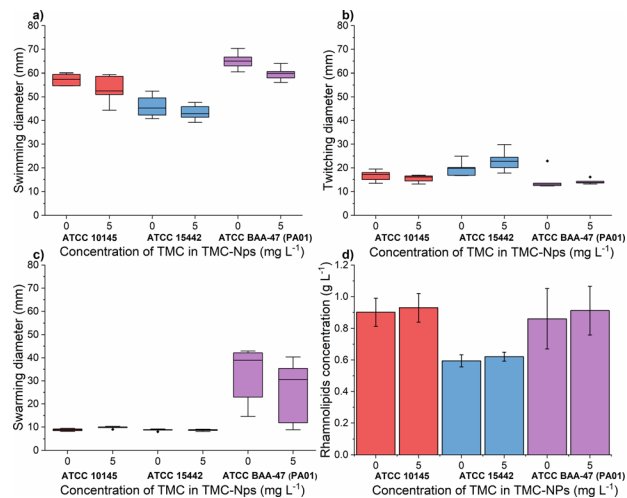
Fig. 7 Effect of sub-MIC TMC-NPs on PA cells ▮ ATCC 10145, ▮ ATCC 15442, and ▮ ATCC BAA-47 (PA01) in comparison to the untreated control, with a focus on (a) swimming motility; (b) twitching motility; (c) swarming motility; and (d) rhamnolipid production. In panels (a–c) dashes indicate the median value. The presented values are a result of duplicate measurements and three independent repetitions.

in the other two strains, the swarming diameter remained small, even in the untreated control. These results suggest that TMC-NPs likely affect flagellar activity, aligning with the concept that swarming motility is primarily driven by flagella, and type IV pili assist the flagellum during surface spreading.[77,78] The reduction in swarming motility as a result of decreased rhamnolipid production after TMC-NP treatment is not supported by our results (see Fig. 7d).

Effect of TMC-NPs' sub-MIC on PA cells' protease activity. PA harbours various proteases crucial for the virulence of this pathogenic bacterium, including alkaline protease AprA, protease IV, and Las elastase.[79] Notably, LasB elastase, the most abundant protein in the secretome, stands out as a key virulence factor demanding attention in the treatment of PA-associated infections. Functional LasB is produced by most PA strains irrespective of their origin[80] and plays a pivotal role in disrupting physical barriers, promoting infection spread, and degrading host immune components.[81] Its significance extends to the development of respiratory infections caused by PA.[82]

A previous study demonstrated the impact of chitosan extracted from the cell wall of *Aspergillus flavus* at a concentration of 100 mg L^{-1} on protease activity, resulting in an almost 60% reduction in the clinical isolate PA.[14] Conversely, a slight decrease was observed in PA (KCTC1637) exposed to chitosan in the concentration range of 32–512 mg L^{-1} (MMW, ≥90% DDA), with no concentration-dependent effect.[63] In our investigation, sub-MIC TMC-NPs did not consistently reduce protease activity across the studied strains (Fig. 8a). A minor reduction in total protease activity was observed only in strain ATCC 10145, where LasB elastase activity was slightly stimulated. In strain ATCC 15442, a modest decrease in LasB elastase activity occurred (Fig. 8b) while preserving total protease activity. The correlation
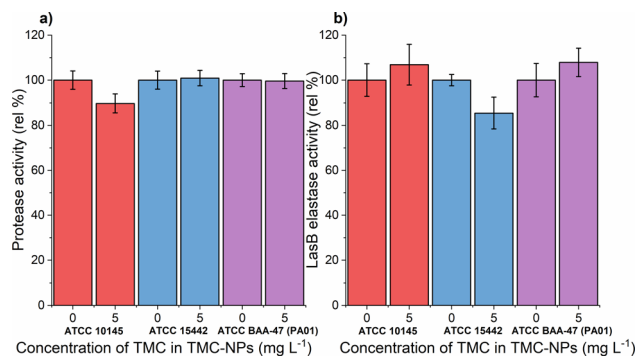
Fig. 8 Effect of sub-MIC TMC-NPs on PA cells ■ ATCC 10145, ■ ATCC 15442, and ■ ATCC BAA-47 (PA01) in comparison to the untreated control, with a focus on (a) protease activity and (b) LasB elastase activity. The presented values are a result of duplicate measurements and three independent repetitions.
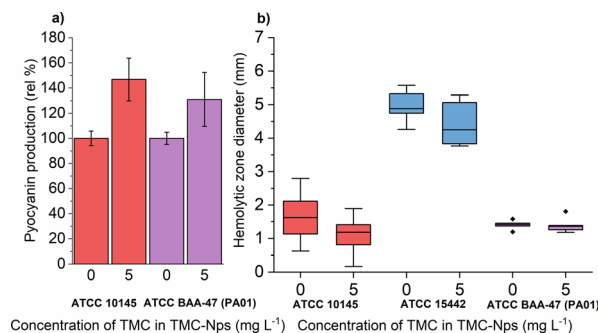

Fig. 9 Effect of sub-MIC TMC-NPs on PA cells ■ ATCC 10145, ■ ATCC 15442, and ■ ATCC BAA-47 (PA01) in comparison to the untreated control, with a focus on (a) pyocyanin production and (b) hemolytic activity. In panel (b) dashes indicate the median value. The presented values are a result of duplicate measurements and three independent repetitions.

between protease activity and quorum sensing (QS) in PA is direct.[83] LasB elastase is under the control of the positive regulator LasR, which serves as the main regulator governing the expression of lasB in an otherwise complex regulatory mechanism.[84,85] Consequently we can hypothesize that the TMC-NPs prepared in our study likely do not disrupt the direct regulatory pathway of QS-dependent proteases. Minor fluctuations in protease activity may be attributed to interactions with secondary transcription regulators or strain-specific factors.[85]

Effect of TMC-NPs' sub-MIC on PA cells' hemolytic activity and pyocyanin production. PA is equipped with two toxins exhibiting hemolytic activity, classified based on their thermostability as heat-resistant and heat-labile hemolysins. The heat-labile form, recognized in the literature as phospholipase C,[86,87] stands out as a virulence factor implicated in various detrimental effects, including paralysis, vascular permeability, footpad swelling, and even lethality in mice upon administration.[88] Furthermore, phospholipase C induces aggregation in human platelets,[89] contributes to lung surfactant dysfunction during infection, and plays a role in severe lung damage.[90]

The production of pyocyanin, another virulence factor, is associated with tissue damage through the generation of reactive oxygen species.[91] Additionally, phenazine compounds present in lung sputum contribute to iron ion reduction (Fe^{3+} → Fe^{2+}) enhancing the availability of iron and absorption in biofilms.[92] Iron is generally a limiting essential element for pathogens during infection since it is sequestered in host organism proteins such as hemoglobin, myoglobin, ferritin, and hemosiderin.[93]

A comparative study revealed that free-form quaternized chitosan was effective against pyocyanin production in three out of four tested strains at 620 mg L^{-1}, with the fourth strain (CVC02118) exhibiting slight overproduction.[52] CS exposure in multiple strains, including PA01, led to decreased pyocyanin levels in a study by Badawy et al.[66] Conversely, our study observed a significant increase in pyocyanin production in both tested strains ATCC 10145 and ATCC BAA-47 (PA01) (note: ATCC 155442 is a strain deficient in pyocyanin production) after exposure to sub-MIC TMC-NPs (Fig. 9a). The increased

pyocyanin production may be a response to the interaction of TMC-NPs with bacterial surfaces, affecting surface charge and extracellular polymeric substance distance from the substratum surface.[94] Attachment of planktonic PA cells to surfaces occurs during the exponential growth phase when cells are phenotypically heterogeneous.[95] Pyocyanin's interaction with eDNA has been shown to influence surface properties, promoting intracellular interactions, aggregation, and biofilm development.[96] Increased pyocyanin production aligns with the observed reduction in FliA activity, a sigma factor regulating bacterial flagellar gene expression, post TMC-NP exposure. However, a study with a mutated FliA demonstrated increased hemolytic activity in PA,[97] which we did not observe (Fig. 9b), probably eliminating pyocyanin overproduction due to flagellar activity disruption.

Experimental

Preparation of CS/TMC-NPs

For the preparation of chitosan (CS) or trimethylchitosan (TMC) nanoparticles (CS/TMC-NPs) *via* the ionic gelation method, we employed CS (LMW 50–190 kDa, 75–85% deacetylated) and TMC chloride (LMW, degree of quaternization >70%), both procured from Sigma-Aldrich. All required solutions were prepared using type I ultrapure water (UPW). To create the CS solution of specific concentrations (0.50; 0.75; 1.00 mg mL^{-1}), chitosan was dissolved overnight (RT; 500 rpm) in acetic acid, the mass concentration of which was 1.5 times higher than that of the chitosan, or in 0.05 M acetate buffer (pH 5). The pH of the chitosan solution was adjusted to 5.0 prior to use. The TMC solution at the concentration 1.00 mg mL^{-1} was prepared through dissolution in UPW. The concentration of TPP crosslinker (purity ≥ 98.0%, Sigma-Aldrich) corresponded to the concentration of CS/TMC used for the reaction and was introduced dropwise into the CS/TMC solution in the required mass ratios $m_{TPP}/m_{CS/TMC}$ (0.43; 0.33; 0.25; 0.20; 0.15; 0.11) under continuous stirring (700 rpm; RT; 30 min). Thus, a solution with a total volume of 10 mL was prepared for subsequent analyses.

Characterisation of CS/TMC-NPs

The mean hydrodynamic size (Z-average), polydispersity index (PDI) and zeta potential of CS/TMC-NPs were determined using a Zetasizer Pro instrument (Malvern Panalytical, UK). Data acquired from the measurements were processed with ZS Explorer software v.2.3.0.62 (Malvern Panalytical, UK). In preparation for the analysis, the samples were standardized to a concentration of 0.1 mg mL^{-1}. Subsequently, NPs loaded into folded capillary zeta cell DTS1070 (Malvern Panalytical, UK) were allowed to equilibrate at 25 °C before the measurement were conducted. Measurements were performed in three independent repetitions.

The morphological characteristics of CS/TMC-NPs were subjected to investigation through electron microscopy. CS-NPs were scrutinized utilizing a 100 kV JEM-1010 TEM (Jeol, JP). Samples were applied onto copper carbon-coated grids and allowed to adhere for several minutes. Excess solution was carefully eliminated by gently tapping the grid on filtration paper, and the affixed samples were further contrasted with a 1% uranyl acetate solution. Subsequently, the grid was inserted into the TEM column and examined at an acceleration voltage of 80 kV under various magnifications. Images were captured using an Olympus SIS MegaView III CCD camera and processed using Analysis v 2.0 software. For the visualization of TMC-NPs, a TEM (EFTEM Jeol 2200 FS, JEOL, JAPAN) was employed, operating at an electron beam energy of 200 kV. A drop of the sample was air-dried when applied to a copper grid and was examined without the application of staining.

The acquired images underwent manual processing utilizing open-source ImageJ software. For each nanoparticle, measurements of the major axis ($2s$) and minor axis ($2b$) were taken, enabling the calculation of the particle's area (A) using eqn (1). This calculated area was then compared with the area determined through a freehand drawing tool. The mean particle diameter was subsequently determined in accordance with eqn (2). Circularity (C) was calculated as the ratio of the particle area (A) to the area of a circle with an equal perimeter (p) (eqn (3)).[98] The particle's perimeter (p) was approximated as outlined in eqn (4). This entire measurement process was repeated for 100 nanoparticles in three separate repetitions.

$$A = \pi ab \qquad (1)$$

$$\overline{d} = \frac{2a + 2b}{2} \qquad (2)$$

$$C = \frac{4\pi A}{p^2} \qquad (3)$$

$$p \approx \pi\sqrt{2\left(a^2 + b^2\right)} \qquad (4)$$

Microorganisms, growth media and conditions

In this work three strains of *Pseudomonas aeruginosa* were used – ATCC 10145, ATCC 15442, and ATCC BAA-47 (PA01). Before antimicrobial tests Luria–Bertani medium (LB – 10 g L^{-1} tryptone, 10 g L^{-1} NaCl, 5 g L^{-1} yeast extract) was inoculated with colonies of PA, which were stored at 4 °C on LB agar plates. The cultivation process was executed over a duration of 24 h at 37 °C with continuous agitation at 150 rpm using orbital shaking.

Antibacterial activity of TMC-NPs against planktonic cells

The assessment of the antibacterial efficacy of TMC-NPs against PA planktonic cells was conducted employing the Bioscreen C microcultivation device (Oy Growth Curves Ab Ltd, Finland) according to Miškovská *et al.*[99] TMC-NPs dispersed in water with a final volume of 70 µl were introduced into a microtiter plate to achieve a final concentration of TMC in TMC-NPs ranging from 5 to 160 mg L^{-1}. Subsequently, 210 µl of LB medium and 30 µl of harvested cells (9000 rcf; RT; 10 min) resuspended in fresh LB medium (OD$_{600}$ of 0.100 ± 0.010) were added to achieve a total volume of 320 µl. Bacterial growth was monitored for 24 h at 37 °C. Each experiment was performed in five parallel and three independent repetitions from which growth curves were generated, and the minimum concentration required to inhibit 50% of bacterial population (MIC$_{50}$) was determined.[99] Additionally, the sub-minimal inhibitory concentration (sub-MIC) was ascertained, representing a concentration that does not impede bacterial growth analogously to Maisetta *et al.*[52]

Activity of TMC-NPs against adhering cells

The assessment of the antibiofilm efficacy of TMC-NPs against PA was carried out in 96-well polystyrene microtiter plates (TPP, CH) according to Michailidu *et al.*[100] TMC-NPs dispersed in water with a final volume of 70 µl were introduced into the wells to achieve a final concentration of TMC in TMC-NPs ranging from 5 to 160 mg L^{-1}. Subsequently, 210 µl of harvested cells (9000 rcf; RT; 10 min) resuspended in fresh LB medium (OD$_{600}$ of 0.800 ± 0.010) were added to attain a total volume of 280 µl. The incubation of the plates was conducted for 24 h at 37 °C with continuous agitation at 150 rpm using orbital shaking. Following incubation, the wells underwent two rounds of washing using an automated microplate washer and dispenser (BioTek 50 TS Washer, USA) with sterile PBS (pH 7.4) to eliminate non-adherent cells. The metabolic activity of adhered cells was evaluated employing the MTT assay, as per the method outlined by Kulišová *et al.*[101] with slight modifications. The washed wells were filled with 60 µl of glucose solution in PBS (57.4 g L^{-1}) and 50 µl of MTT solution in PBS (1.0 g L^{-1}) and incubated for 60 min at 37 °C with continuous shaking at 150 rpm. Following incubation, a solvent solution (pH 4.7) composed of 160 g L^{-1} SDS, 400 g L^{-1} DMF, and 20 g L^{-1} acetic acid, diluted in PBS (pH 7.4), was added to dissolve coloured formazan crystals. The plates were again incubated for 30 min at 37 °C with agitation at 230 rpm, and 100 µl aliquots were analysed at 570 nm using a UV-Vis spectrophotometer, Infinite M200 Pro reader (Tecan, CH). Each experiment was performed in eight parallel and three independent repetitions from which the minimum biofilm inhibiting concentration required to reduce biofilm development by 50% (MBIC$_{50}$) was determined,

in comparison to the nanoparticle-free control, which was assigned to be 100%.

Effect of TMC-NPs on virulence of PA

All assessments were conducted at a sub-MIC of TMC-NPs, specifically at 5 mg L^{-1}, a concentration determined not to impact the growth kinetics of PA. This precaution was taken to prevent any inadvertent influence on virulence resulting from a reduction in cell numbers during experiment performance. Each experiment was carried out in duplicate, with three independent repetitions. The treatment protocol for PA cells with TMC-NPs mirrored the approach employed for determining the antibacterial activity of TMC-NPs against planktonic cells, albeit with specific modifications. In the case of agar plate methods, the LB medium, utilized for the resuspension and dilution of PA cells, was substituted with sterile phosphate buffer (pH 7.4). Following a one-hour incubation period (37 °C, 150 rpm) in the presence of TMC-NPs, agar plates were inoculated with 10 μl of the cell suspension. The remaining methods were executed in a 40× larger volume, and the resuspended cells in phosphate buffer (OD$_{600}$ of 0.100 ± 0.010) were incubated for 24 hours (37 °C, 150 rpm) in the presence of LB media. For the determination of rhamnolipids, the LB medium was replaced with a basic mineral medium (3.4 g L^{-1} KH$_2$PO$_4$, 4.4 g L^{-1} K$_2$HPO$_4$, 15.0 g L^{-1} NaNO$_3$, 1.1 g L^{-1} KCl, 1.1 g L^{-1} NaCl, 0.5 g L^{-1} yeast extract, 20.0 g L^{-1} sodium citrate, 0.224 g L^{-1} MgSO$_4$, 0.28 mg L^{-1} FeSO$_4$·7H$_2$O, 1.45 mg L^{-1} ZnSO$_4$·7H$_2$O, 1.25 mg L^{-1} CuSO$_4$·5H$_2$O, 8.40 mg L^{-1} MnSO$_4$·H$_2$O, 1.20 mg L^{-1} CaCl$_2$·4H$_2$O). Given that all other methodologies were predicated on the monitoring of extracellular products, the supernatant from free cells (9000 rcf; RT; 10 min) was utilized for subsequent assessments.

Motility assays. Motility assessments were conducted following the methodology outlined by Saeki et al.[102] Agar plates designed for detecting swimming (10 g L^{-1} tryptone, 5 g L^{-1} NaCl, 3 g L^{-1} bacteriological agar) and swarming motility (10 g L^{-1} D-glucose, 5 g L^{-1} peptone, 2 g L^{-1} yeast extract, 5 g L^{-1} bacteriological agar) were inoculated with a cell suspension on the agar surface. Incubation occurred for 24 hours at 37 °C without plate inversion. For twitching motility, the suspension was applied to the bottom of the agar and incubated for 24 hours at 37 °C with inversion. The motility zones were measured using ImageJ software.

Hemolysis assay. The determination of hemolytic activity followed the protocol established by Lo et al.[97] with some modifications. Blood agar (20 g L^{-1} peptone, 5 g L^{-1} NaCl, 5% v/v defibrinated sheep blood, 15 g L^{-1} bacteriological agar) was inoculated with a cell suspension at the bottom. Plates were incubated with inversion for 48 hours at 37 °C, after which the hemolytic zone was measured using ImageJ software.

Rhamnolipid determination. The quantification of rhamnolipids was carried out using the phenol–sulfur method with rhamnose as a standard, following the procedure described by Maťátková et al.[103] One milliliter of cell-free supernatant (diluted 20×) was mixed with 1 mL of 5% (w/w) phenol solution and 5 mL of concentrated sulfuric acid. After a 30 min

incubation at room temperature (RT), 200 μl aliquots were analyzed at 490 nm using a UV-Vis spectrophotometer, Infinite M200 Pro reader (Tecan, CH).

Pyocyanin determination. The assessment of pyocyanin production was determined according to Kašparová et al.[104] Strain ATCC 15442, which is pyocyanin-deficient, was employed as a negative control. Two milliliters of cell-free supernatant were mixed with 1.6 mL of chloroform (Penta, CZ). After mixing, 1 mL of the chloroform phase was mixed with 0.5 mL of 1 M hydrochloric acid (Penta, CZ). Upper phase aliquots of 200 μl were analyzed at 520 nm using a UV-Vis spectrophotometer, Infinite M200 Pro reader (Tecan, CH).

Protease activity determination. Protease activity was determined following the procedure outlined by Das et al.[105] A cell-free supernatant of 150 μl was mixed with 1 mL of azocasein (3 g L^{-1}, Sigma-Aldrich, USA) solution in 50 mM Tris HCl buffer (pH 8, PanReac AppliChem, DE). After mixing, the samples were incubated for 15 min at 37 °C and 150 rpm, after which 500 μl of 10% (w/w) trichloroacetic acid (Penta, CZ) was added. The resulting precipitate was separated (5 min, 10 000 rpm), and 200 μl aliquots were analyzed at 400 nm using a UV-Vis spectrophotometer, Infinite M200 Pro reader (Tecan, CH).

LasB elastase activity determination. LasB elastase activity was assessed following the protocol outlined by Ziuzina et al.[106] A cell-free supernatant of 700 μl was combined with 250 μl of elastin conjugated with Congo red (5 g L^{-1}, Sigma-Aldrich, USA) in 1 M Tris HCl buffer (pH 8, PanReac AppliChem, DE). After thorough mixing, the samples underwent a 24 hour incubation at 150 rpm and 37 °C, following which 200 μl aliquots of the supernatant (13 000 rpm, 10 min) were analyzed at 495 nm using a UV-Vis spectrophotometer, Infinite M200 Pro reader (Tecan, CH).

Conclusions

In this study, we investigated the antimicrobial capacity of chitosan nanoparticles (CS-NPs), with a specific emphasis on combatting the biofilm-forming pathogenic bacterium PA. The synthesis of CS-NPs was achieved through ionic gelation utilizing trivalent TPP anions, with subsequent characterization of the resulting nanoparticles regarding size, charge, and stability. While nanoparticles from two different types of chitosan were successfully prepared, namely CS-NPs (median size 30 nm, circularity 0.986) and TMC-NPs (median size 103 nm, circularity 0.967), CS-NPs were excluded from antimicrobial testing. This exclusion was caused by aggregation in culture media which implies a broader usability of quaternized CS TMC-NPs.

Our prepared TMC-NPs, exhibiting favourable characteristics for biomedical applications, including nanoscale size, regular spherical morphology, and stability in water and complex culture media, were evaluated for their antimicrobial activity against PA through MIC and sub-MIC determination. Notably, TMC-NPs demonstrated efficacy at a low concentration (MIC$_{50}$ ≥ 160 mg L^{-1}) compared to existing literature focusing on the antipseudomonal activity of free-form chitosan. However, due to this promoted efficacy the sub-MIC value of

TMC-NPs was found at a low concentration (5 mg L^{-1}) and at this concentration we observed a reduction in PA hemolytic activity and motility (swarming, swimming). Importantly, TMC-NPs emerged as a more effective antibiofilm agent (MBIC$_{50}$ 80–160 mg L^{-1}) than disruptors of planktonic growth, suggesting their potential as supportive agents in combating PA biofilm development. Nevertheless, it is imperative to highlight the increased production of pyocyanin as a PA response to the influence of sub-MIC TMC-NPs. We attribute this observation to PA compensating for reduced adhesion efficiency. This statement requires further investigation to elucidate the proposed mechanism.

In summary, our study demonstrates the synthesis conditions for TMC-NPs with properties conducive to biomedical applications. Moreover, it underscores the potential of TMC-NPs as an antipseudomonal agent and demonstrates the beneficial effects of CS methylation and the conversion of TMC into nanoparticles in enhancing the antimicrobial activity of CS, as compared to relevant literature. With the well-established safety profile of TMC, our TMC-NPs could be strategically utilized in combination with other antimicrobial agents to enhance efficacy. Additionally, our comprehensive screening of TMC-NPs against key virulence factors of PA reveals their capacity in combating PA infections. This suggests a possible role for TMC-NPs as adjunctive therapy in infections caused by this pathogen, with their primary benefit likely lying in modulating biofilm formation. Further work should focus on the specific formulation of TMC-NPs and expand screening testing to include additional bacterial strains, thus increasing the prospect of chitosan in antimicrobial applications.

Author contributions

Conceptualization, D. M.; data curation, D. M., A. K.; formal analysis, D. M., A. K.; funding acquisition, D. M., J. M.; investigation, D. M., O. M., J. M.; methodology, D. M., O. M.; project administration, D. M., J. M.; resources, O. M., J. M.; supervision, J. M.; writing – original draft, D. M., writing – review & editing, O. M., J. M.

Conflicts of interest

There are no conflicts to declare.

Acknowledgements

Notes and references

1 J. Frigaard, J. L. Jensen, H. K. Galtung and M. Hiorth, *Front. Pharmacol*, 2022, **13**, 880377.

2 R. Y. Pelgrift and A. J. Friedman, *Adv. Drug Delivery Rev.*, 2013, **65**, 1803–1815.

3 M. A. Mohammed, J. T. M. Syeda, K. M. Wasan and E. K. Wasan, *Pharmaceutics*, 2017, **9**(4), 53.

4 U. Garg, S. Chauhan, U. Nagaich and N. Jain, *Adv. Pharm. Bull.*, 2019, **9**, 195–204.

5 S. K. R. Namasivayam, U. K. Pandian, K. Samrat, R. S. Arvind Bharani, A. John, M. Kavisri, S. Kadaikunnan, M. Thiruvengadam and M. Moovendhan, *Int. J. Biol. Macromol.*, 2024, **259**, 129264.

6 S. Karthick Raja Namasivayam, V. Pattukumar, K. Samrat, J. A. Kumar, R. S. Arvind Bharani, A. A. Alothman, S. M. Osman, V. A. Tran and M. Rajasimman, *Chemosphere*, 2022, **308**, 135950.

7 S. Karthick Raja Namasivayam, R. S. Arvind Bharani and K. Karunamoorthy, *Int. J. Biol. Macromol.*, 2018, **120**, 921–944.

8 S. K. Raja Namasivayam, G. Venkatachalam and R. S. Arvind Bharani, *Sustainable Chem. Pharm.*, 2020, **17**, 100300.

9 A. Verlee, S. Mincke and C. V. Stevens, *Carbohydr. Polym.*, 2017, **164**, 268–283.

10 R. Fattah, F. Fathy, T. A. H. Mohamed and M. S. Elsayed, *AIMS Microbiol.*, 2021, **7**, 415–430.

11 R. Ikono, E. Mardliyati, I. T. Agustin, M. M. F. Ulfi, D. Andrianto, U. Hasanah, B. M. Bachtiar, N. Mardianingsih, E. W. Bachtiar and N. N. Maulana, *Biomed. Phys. Eng. Express*, 2018, **4**, 045026.

12 J. P. Horcajada, M. Montero, A. Oliver, L. Sorlí, S. Luque, S. Gómez-Zorrilla, N. Benito and S. Grau, *Clin. Microbiol. Rev.*, 2019, **32**(4), e00031.

13 P. Piewngam, J. Chiou, P. Chatterjee and M. Otto, *Expert Rev. Anti-Infect. Ther.*, 2020, **18**, 499–510.

14 S. N. Muslim, I. Kadmy, A. N. M. Ali, B. K. Salman, M. Ahmad, S. S. Khazaal, N. H. Hussein and S. N. Muslim, *Int. J. Biol. Macromol.*, 2018, **107**, 52–58.

15 M. Whiteley, S. P. Diggle and E. P. Greenberg, *Nature*, 2017, **551**, 313–320.

16 G. Tommonaro, *Quorum Sensing: Molecular Mechanism and Biotechnological Application*, Academic Press, 2019.

17 G. A. O'Toole and R. Kolter, *Mol. Microbiol.*, 1998, **30**, 295–304.

18 P. Rivera Aguayo, T. Bruna Larenas, C. Alarcón Godoy, B. Cayupe Rivas, J. González-Casanova, D. Rojas-Gómez and N. Caro Fuentes, *Antibiotics*, 2020, **9**(9), 551.

19 T. A. Ahmed and B. M. Aljaeid, *Drug Des., Dev. Ther.*, 2016, **10**, 483–507.

20 P. Calvo, C. Remuñán-López, J. L. Vila-Jato and M. J. Alonso, *J. Appl. Polym. Sci.*, 1997, **63**, 125–132.

21 K. Songsurang, N. Praphairaksit, K. Siraleartmukul and N. Muangsin, *Arch. Pharmacal Res.*, 2011, **34**, 583–592.

22 Y.-H. Lin, K. Sonaje, K. M. Lin, J.-H. Juang, F.-L. Mi, H.-W. Yang and H.-W. Sung, *J. Controlled Release*, 2008, **132**, 141–149.

23 M. C. Di Santo, C. L. D' Antoni, A. P. Domínguez Rubio, A. Alaimo and O. E. Pérez, *Biomed. Pharmacother.*, 2021, **142**, 111970.

24 H. Liu and C. Gao, *Polym. Adv. Technol.*, 2009, **20**, 613–619.

25 S. Vaezifar, S. Razavi, M. A. Golozar, S. Karbasi, M. Morshed and M. Kamali, *J. Cluster Sci.*, 2013, **24**, 891–903.
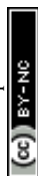
26 E. N. Koukaras, S. A. Papadimitriou, D. N. Bikiaris and G. E. Froudakis, *Mol. Pharm.*, 2012, **9**, 2856–2862.

27 H. Jonassen, A.-L. Kjøniksen and M. Hiorth, *Colloid Polym. Sci.*, 2012, **290**, 919–929.

28 S. Sreekumar, F. M. Goycoolea, B. M. Moerschbacher and G. R. Rivera-Rodriguez, *Sci. Rep.*, 2018, **8**, 4695.

29 H.-C. Yang and M.-H. Hon, *Microchem. J.*, 2009, **92**, 87–91.

30 W. Fan, W. Yan, Z. Xu and H. Ni, *Colloids Surf., B*, 2012, **90**, 21–27.

31 R. Sánchez-Clemente, M. I. Igeño, A. G. Población, M. I. Guijo, F. Merchán and R. Blasco, *Proceedings*, 2018, **2**, 1297.

32 K. Ozturk, F. B. Arslan, E. Tavukcuoglu, G. Esendagli and S. Calis, *Int. J. Pharm.*, 2020, **578**, 119119.

33 M. Thanou, J. C. Verhoef and H. E. Junginger, *Adv. Drug Delivery Rev.*, 2001, **52**, 117–126.

34 J. Cho, M.-C. Heuzey, A. Bégin and P. J. Carreau, *J. Food Eng.*, 2006, **74**, 500–515.

35 M. L. Tsaih and R. H. Chen, *Int. J. Biol. Macromol.*, 1997, **20**, 233–240.

36 N. Sawtarie, Y. Cai and Y. Lapitsky, *Colloids Surf., B*, 2017, **157**, 110–117.

37 S. Bhattacharjee, *J. Controlled Release*, 2016, **235**, 337–351.

38 T. Kiang, J. Wen, H. W. Lim and K. W. Leong, *Biomaterials*, 2004, **25**, 5293–5301.

39 A. Geçer, N. Yıldız, A. Çalımlı and B. Turan, *Macromol. Res.*, 2010, **18**, 986–991.

40 B. Sayın, S. Somavarapu, X. W. Li, M. Thanou, D. Sesardic, H. O. Alpar and S. Şenel, *Int. J. Pharm.*, 2008, **363**, 139–148.

41 B. L. Banik, P. Fattahi and J. L. Brown, *Wiley Interdiscip. Rev.: Nanomed. Nanobiotechnol.*, 2016, **8**, 271–299.

42 H. Rauscher, B. Sokull-Klüttgen and H. Stamm, *Nanotoxicology*, 2013, **7**, 1195–1197.

43 M. Müsken, S. Di Fiore, U. Römling and S. Häussler, *Nat. Protoc.*, 2010, **5**, 1460–1469.

44 T. López-León, E. L. S. Carvalho, B. Seijo, J. L. Ortega-Vinuesa and D. Bastos-González, *J. Colloid Interface Sci.*, 2005, **283**, 344–351.

45 M. Tré-Hardy, F. Vanderbist, H. Traore and M. J. Devleeschouwer, *Int. J. Antimicrob. Agents*, 2008, **31**, 329–336.

46 J. Lee and L. Zhang, *Protein Cell*, 2015, **6**, 26–41.

47 N. Boudouaia, M. L. Benine, N. Fettal, B. Abbouni and Z. Bengharez, *Waste Biomass Valorization*, 2023, **15**, 1267–1279.

48 Y. Hu, Y. Du, J. Yang, Y. Tang, J. Li and X. Wang, *Polymer*, 2007, **48**, 3098–3106.

49 S. Tin, K. R. Sakharkar, C. S. Lim and M. K. Sakharkar, *Int. J. Biol. Sci.*, 2009, **5**, 153–160.

50 Y. Liu, Y. Jiang, J. Zhu, J. Huang and H. Zhang, *Carbohydr. Polym.*, 2019, **206**, 412–419.

51 S. Rathinam, S. Ólafsdóttir, S. Jónsdóttir, M. Á. Hjálmarsdóttir and M. Másson, *Int. J. Biol. Macromol.*, 2020, **160**, 548–557.

52 G. Maisetta, A. M. Piras, V. Motta, S. Braccini, D. Mazzantini, F. Chiellini, Y. Zambito, S. Esin and G. Batoni, *Microorganisms*, 2021, **9**(5), 912.

53 N. A. Melake, H. A. Mahmoud and M. T. Al-Semary, *Afr. J. Microbiol. Res.*, 2012, **6**, 5387–5398.

54 A. Salis, M. Fanti, L. Medda, V. Nairi, F. Cugia, M. Piludu, V. Sogos and M. Monduzzi, *ACS Biomater. Sci. Eng.*, 2016, **2**, 741–751.

55 D. B. Martins, F. D. Nasário, L. C. Silva-Gonçalves, V. A. de Oliveira Tiera, M. Arcisio-Miranda, M. J. Tiera and M. P. dos Santos Cabrera, *Carbohydr. Polym.*, 2018, **181**, 1213–1223.

56 F. Chen, Z.-R. Zhang, F. Yuan, X. Qin, M. Wang and Y. Huang, *Int. J. Pharm.*, 2008, **349**, 226–233.

57 T. Kean, S. Roth and M. Thanou, *J. Controlled Release*, 2005, **103**, 643–653.

58 J. W. Hickey, J. L. Santos, J. M. Williford and H. Q. Mao, *J. Controlled Release*, 2015, **219**, 536–547.

59 F. Dilnawaz, S. Acharya and A. Kanungo, *Polym. Bull.*, 2024, **81**, 1071–1095.

60 M. Chandrasekaran, K. D. Kim and S. C. Chun, *Processes*, 2020, **8**(9), 1173.

61 D. Yan, Y. Li, Y. Liu, N. Li, X. Zhang and C. Yan, *Molecules*, 2021, **26**(23), 7136.

62 A. M. Piras, S. Esin, A. Benedetti, G. Maisetta, A. Fabiano, Y. Zambito and G. Batoni, *Int. J. Mol. Sci.*, 2019, **20**, 6297.

63 F. Khan, P. Manivasagan, D. T. N. Pham, J. Oh, S.-K. Kim and Y.-M. Kim, *Microb. Pathog.*, 2019, **128**, 363–373.

64 P. Rivera Aguayo, T. Bruna Larenas, C. Alarcón Godoy, B. Cayupe Rivas, J. González-Casanova, D. Rojas-Gómez and N. Caro Fuentes, *Antibiotics*, 2020, **9**, 551.

65 D. Rubini, S. F. Banu, P. Subramani, B. N. V. Hari, S. Gowrishankar, S. K. Pandian, A. Wilson and P. Nithyanand, *Pathog. Dis.*, 2019, **77**, ftz009.

66 M. S. E. M. Badawy, O. K. M. Riad, F. A. Taher and S. A. Zaki, *Int. J. Biol. Macromol.*, 2020, **149**, 1109–1117.

67 R. Thaya, B. Vaseeharan, J. Sivakamavalli, A. Iswarya, M. Govindarajan, N. S. Alharbi, S. Kadaikunnan, M. N. Al-anbr, J. M. Khaled and G. Benelli, *Microb. Pathog.*, 2018, **114**, 17–24.

68 D.-G. Ha, S. L. Kuchma and G. A. O'Toole, *Pseudomonas Methods and Protocols*, 2014, 59–65.

69 M. Bouteiller, C. Dupont, Y. Bourigault, X. Latour, C. Barbey, Y. Konto-Ghiorghi and A. Merieau, *Int. J. Mol. Sci.*, 2021, **22**(7), 3337.

70 S. Zhu, M. Schniederberend, D. Zhitnitsky, R. Jain, J. E. Galán, B. I. Kazmierczak and J. Liu, *J. Bacteriol.*, 2019, **201**(13), e00117.

71 W. Wu, Y. Jin, F. Bai and S. Jin, in *Molecular Medical Microbiology*, ed. Y.-W. Tang, M. Sussman, D. Liu, I. Poxton and J. Schwartzman, Academic Press, Boston, 2nd edn, 2015, pp. 753–767, DOI: 10.1016/B978-0-12-397169-2.00041-X.

72 M. J. Kühn, L. Talà, Y. F. Inclan, R. Patino, X. Pierrat, I. Vos, Z. Al-Mayyah, H. Macmillan, J. Negrete, J. N. Engel and A. Persat, *Proc. Natl. Acad. Sci. U. S. A.*, 2021, **118**, e2101759118.

73 J. Tremblay and E. Déziel, *BMC Genomics*, 2010, **11**, 587.

74 A. Yang, W. S. Tang, T. Si and J. X. Tang, *Biophys. J.*, 2017, **112**, 1462–1471.

75 J. Overhage, S. Lewenza, A. K. Marr and R. E. Hancock, *J. Bacteriol.*, 2007, **189**, 2164–2169.

76 N. C. Caiazza, R. M. Q. Shanks and G. A. O'Toole, *J. Bacteriol.*, 2005, **187**, 7351–7361.

77 T. S. Murray and B. I. Kazmierczak, *J. Bacteriol.*, 2008, **190**, 2700–2708.

78 T. Köhler, K. Curty Lasta, F. Barja, C. van Delden and J.-C. Pechère, *J. Bacteriol.*, 2000, **182**, 5990–5996.

79 S. Bleves, V. Viarre, R. Salacha, G. P. F. Michel, A. Filloux and R. Voulhoux, *Int. J. Med. Microbiol.*, 2010, **300**, 534–543.

80 A. Llanos, P. Achard, J. Bousquet, C. Lozano, M. Zalacain, C. Sable, H. Revillet, M. Murris, M. Mittaine, M. Lemonnier and M. Everett, *Sci. Rep.*, 2023, **13**, 14208.

81 M. Mateu-Borrás, L. Zamorano, A. González-Alsina, I. Sánchez-Diener, A. Doménech-Sánchez, A. Oliver and S. Albertí, *Front. Cell. Infect. Microbiol.*, 2022, **11**, 816356.

82 F. Bastaert, S. Kheir, V. Saint-Criq, B. Villeret, P. M. Dang, J. El-Benna, J. C. Sirard, R. Voulhoux and J. M. Sallenave, *Front. Immunol.*, 2018, **9**, 1675.

83 S. P. Diggle, A. S. Griffin, G. S. Campbell and S. A. West, *Nature*, 2007, **450**, 411–414.

84 Y. Wang, L. Gao, X. Rao, J. Wang, H. Yu, J. Jiang, W. Zhou, J. Wang, Y. Xiao, M. Li, Y. Zhang, K. Zhang, L. Shen and Z. Hua, *Sci. Rep.*, 2018, **8**, 13344.

85 M. J. Everett and D. T. Davies, *Drug Discovery Today*, 2021, **26**, 2108–2123.

86 R. M. Berka and M. L. Vasil, *J. Bacteriol.*, 1982, **152**, 239–245.

87 L. R. Montes, M. Ibarguren, F. M. Goñi, M. Stonehouse, M. L. Vasil and A. Alonso, *Biochim. Biophys. Acta*, 2007, **1768**, 2365–2372.

88 R. S. Berk, D. Brown, I. Coutinho and D. Meyers, *Infect. Immun.*, 1987, **55**, 1728–1730.

89 I. R. Coutinho, R. S. Berk and E. Mammen, *Thromb. Res.*, 1988, **51**, 495–505.

90 M. J. Wargo, M. J. Gross, S. Rajamani, J. L. Allard, L. K. Lundblad, G. B. Allen, M. L. Vasil, L. W. Leclair and D. A. Hogan, *Am. J. Respir. Crit. Care Med.*, 2011, **184**, 345–354.

91 S. Hall, C. McDermott, S. Anoopkumar-Dukie, A. J. McFarland, A. Forbes, A. V. Perkins, A. K. Davey, R. Chess-Williams, M. J. Kiefel, D. Arora and G. D. Grant, *Toxins*, 2016, **8**(8), 236.

92 P. Cornelis and J. Dingemans, *Front. Cell. Infect. Microbiol.*, 2013, **3**, 75.

93 J. Bullen, *Rev. Infect. Dis.*, 1981, **3**, 1127–1138.

94 N. P. Boks, W. Norde, H. C. van der Mei and H. J. Busscher, *Microbiology*, 2008, **154**, 3122–3133.

95 S. Yang, X. Cheng, Z. Jin, A. Xia, L. Ni, R. Zhang and F. Jin, *Appl. Environ. Microbiol.*, 2018, **84**, e00700–e00718.

96 T. Das, S. K. Kutty, N. Kumar and M. Manefield, *PLoS One*, 2013, **8**, e58299.

97 Y.-L. Lo, C.-L. Chen, L. Shen, Y.-C. Chen, Y.-H. Wang, C.-C. Lee, L.-C. Wang, C.-H. Chuang, R. P. Janapatla, C.-H. Chiu and H.-Y. Chang, *Res. Microbiol.*, 2018, **169**, 135–144.

98 S. J. BLOTT and K. PYE, *Sedimentology*, 2008, **55**, 31–63.

99 A. Mišková, M. Rabochová, J. Michailidu, J. Masák, A. Čejková, J. Lorinčík and O. Maťátková, *PLoS One*, 2022, **17**, e0272844.

100 J. Michailidu, O. Maťátková, I. Kolouchová, J. Masák and A. Čejková, *Plants*, 2022, **11**(3), 443.

101 M. Kulišová, O. Maťátková, T. Brányik, J. Zelenka, L. Drábová and I. J. Kolouchová, *J. Microbiol. Methods*, 2023, **205**, 106676.

102 E. K. Saeki, A. Y. Yamada, L. A. de Araujo, L. Anversa, D. d. O. Garcia, R. L. B. de Souza, H. M. Martins, R. K. T. Kobayashi and G. Nakazato, *Front. Cell. Infect. Microbiol.*, 2021, **11**, 656984.

103 O. Maťátková, J. Michailidu, R. Ježdík, I. Jarošová Kolouchová, T. Řezanka, V. Jirků and J. Masák, *Microorganisms*, 2022, **10**, 1272.

104 P. Kašparová, E. Vaňková, M. Paldrychová, A. Svobodová, R. Hadravová, I. Jarošová Kolouchová, J. Masák and V. Scholtz, *Front. Cell. Infect. Microbiol.*, 2022, **12**, 993029.

105 M. C. Das, P. Sandhu, P. Gupta, P. Rudrapaul, U. C. De, P. Tribedi, Y. Akhter and S. Bhattacharjee, *Sci. Rep.*, 2016, **6**, 23347.

106 D. Ziuzina, D. Boehm, S. Patil, P. J. Cullen and P. Bourke, *PLoS One*, 2015, **10**, e0138209.